Available online at www.sciencedirect.com
ScienceDirect
Continental Shelf Research 27 (2007) 1528–1547
CONTINENTAL SHELF RESEARCH
www.elsevier.com/locate/csr

Flow structure at a trifurcation near a North Florida inlet

Bret M. Webb*, Jeffrey N. King, Bilge Tutak, Arnoldo Valle-Levinson

Department of Civil & Coastal Engineering, University of Florida, Gainesville, FL 32611-6590, USA

Received 23 August 2006; received in revised form 12 January 2007; accepted 17 January 2007
Available online 6 February 2007

Abstract

Barrier island estuarine systems are common along the East and Gulf coasts of Florida. While some information regarding these systems is available in report form, detailed observational studies of their hydrodynamic properties are scarce in existing literature. Hydrography and current velocity were observed at a tidally driven coastline trifurcation, adjacent to the St. Augustine Inlet, Florida, in the Guana–Tolomato–Matanzas Estuary. Data were collected over nearly a semidiurnal period on February 2, 2006. The domain is well mixed and convergence fronts appear aligned with bathymetry. Eighty-six percent of the tidal variability in the study area is explained by the semidiurnal harmonic, which propagates through the system as a quasi-standing wave. The mean flow structure at the inlet (inflow in channel and outflow over shoals) governs intra-estuarine communication and is consistent with theoretical residual flows produced by a standing tidal wave. The governing force balance is between advective acceleration and the barotropic pressure gradient. The mean flow structure across the inlet might be explained by both Li and O'Donnell's [2005. The effect of channel length on the residual circulation in tidally dominated channels. Journal of Physical Oceanography 35, 1826–1840] analytical model, and Stommel and Farmer's [1952. On the nature of estuarine circulation. Woods Hole Oceanographic Institute, Woods Hole, Massachusetts, Ref. 52–51, 52–63, 52–88] source–sink analog. Flow characteristics for St. Augustine Inlet are compared with Beaufort Inlet, North Carolina; North Inlet, South Carolina; and Sand Shoal Inlet, Virginia. While these systems share similar characteristics, a common subtidal flow structure is not evident.

Keywords: Florida; Guana; Tolomato; Matanzas; St. Augustine; Inlet; Estuary; Mean flow; Residual circulation

1. Introduction

The region between Cape Hatteras, North Carolina and the Florida Keys—in the eastern United States of America—is dominated by coastal plain, piedmont, and bar-built estuarine systems (Dame et al., 2000). In some of these systems, tidal flood-flows split in two or more directions on the estuary side of the inlets. For example, on the estuary side of St. Augustine Inlet (Fig. 1) flood-flows split into one of three tributaries at a trifurcation. The governing hydrodynamics in tidally driven, split-flow regions in the vicinity of inlets (inlet-proximate) do not always fit classical models, like Pritchard (1956) or Hansen and Rattray (1966). This is especially true of systems that lack stratification and yet exhibit lateral variations in the subtidal flow.

The structure of inlet-proximate, tidally driven split flows has been described with observations in a

*Corresponding author. Tel.: +1 352 392 9537x1414; fax: +1 352 392 7343.
E-mail addresses: bwebb@coastal.ufl.edu (B.M. Webb), jeffrey.n.king@gmail.com (J.N. King), tutak@coastal.ufl.edu (B. Tutak), arnoldo@coastal.ufl.edu (A. Valle-Levinson).

0278-4343/$ - see front matter
doi:10.1016/j.csr.2007.01.021

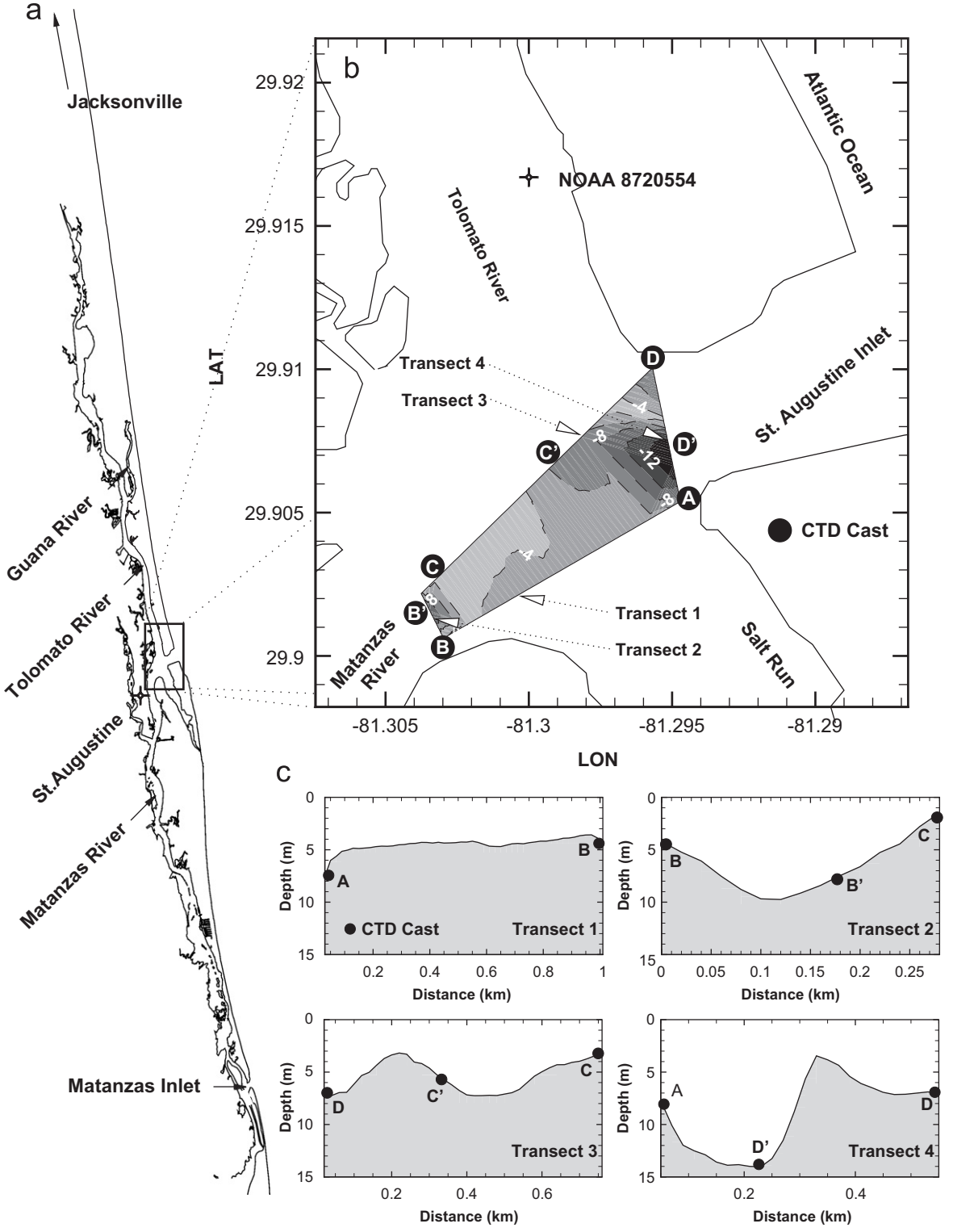

Fig. 1. (a) The Northeast Florida coastline, (b) the study area, and (c) the average bathymetry for each transect. Black dots in (b) and (c) denote cast locations around the sampling circuit. Triangulated bathymetry is contoured (interval = 2 m) within the study domain with dark colors representing deeper areas, and lighter colors depicting shallower areas.

few systems. For example, Kjerfve and Proehl (1979), Kjerfve et al. (1981), Kjerfve et al. (1982), Dame et al. (1986), and Kjerfve et al. (1991) described North Inlet, South Carolina, USA; Churchill et al. (1999) and Hench and Luettich (2003) studied Beaufort Inlet, North Carolina, USA; and Li (2002) characterized Sand Shoal Inlet, Virginia, USA. These studies show that the residual circulation pattern at each inlet is unique, even though these inlets share some characteristics, such as tidal dominance and homogeneous hydrography.

Exchange flows in estuaries may be the result of horizontal density gradients, wind forcing, tidal rectification, or a combination of these influences. Wong (1994); Winant (2004), and Sanay and Valle-Levinson (2005) show that exchange flows might occur in response to wind, such that a down-estuary wind will cause inflow in the channel and outflow over the shoals. Kasai et al. (2000) and Valle-Levinson et al. (2003) show that density-induced flows exhibit inflow in the channel and outflow over the shoals, when influenced by friction (high Ekman number: the ratio of friction forces to Coriolis force). This is consistent with the results of Fischer (1972) and Wong (1994). Under weak friction (low Ekman number) inflow occurs near the channel bed and over the right shoal (looking into the estuary in the northern hemisphere), and outflow occurs near the channel surface and over the left shoal. Li and O'Donnell (2005) show, with an analytical model, that tidally induced exchange flows might be a function of a dimensionless channel length parameter

$$\delta = \frac{4L}{\lambda}, \tag{1}$$

where L is dimensional channel length, λ is the wavelength ($\lambda = \sqrt{gH}/\sigma$), g is gravitational acceleration, H is depth, and σ is tidal frequency. For short channels ($\delta < 0.6$) inflow develops in the channel and outflow occurs over the shoals; the pattern is reversed for long channels. The analytical model of Li and O'Donnell (2005) requires no density stratification, negligible Coriolis acceleration, and a primary subtidal momentum balance between advective acceleration or friction, and the barotropic pressure gradient. The lateral variability of subtidal flow predicted by the Li and O'Donnell (2005) model, for a short channel, is consistent with observations made by Winant and Gutiérrez de Velasco (2003) and predicted by the model of Zimmerman (1981).

Tidal exchange at an estuarine-inlet system might also be characterized by an ebb-flood asymmetry, similar to the potential flow theory of Stommel and Farmer (1952), where ebb flow evacuates the estuary as a seaward-directed jet, or source, while flood flow is drawn into the system as a radial sink. This source–sink analog is often referred to as "tidal pumping" (Fischer et al., 1979) and describes the horizontal or vertical exchange of estuary and ocean water near an inlet (Chadwick and Largier, 1999).

The objective of this study is to characterize causal relationships between forcing mechanisms and flow structure at inlet-proximate, tidally driven splits. To address this objective, velocity and hydrography were sampled west of St. Augustine Inlet, Florida, in the Guana–Tolomato–Matanzas Estuary.

2. Study area and atmospheric conditions

The 60-km-long Guana–Tolomato–Matanzas Estuary is located south of Jacksonville, on Florida's northeast Atlantic coast (Fig. 1). The estuary contains no sizable embayment, and is comprised of three main tributaries: the Guana River, the Tolomato River, and the Matanzas River. Numerous minor tributaries drain to these main tributaries. Main tributary widths are typically less than 500 m, and rarely exceed 1 km. The tidal range in the St. Augustine Inlet is typically between 1.3 m and 1.5 m (NOAA, 2006). The estuary connects to the Atlantic Ocean through two inlets: the St. Augustine Inlet on the east boundary of the study area, and the Matanzas Inlet approximately 25 km to the south. Weather conditions at the Guana–Tolomato–Matanzas National Estuarine Research Reserve weather station during the sampling period (Fig. 2) were such that atmospheric forcing played a negligible role on circulation, as detailed in Section 5. The station did not record any precipitation during the study period.

3. Data collection and processing

Underway velocity profiles and surface temperature and salinity data were combined with profiles of temperature and salinity at fixed points to determine patterns of residual circulation. Data were collected on February 2, 2006 between 1200 and 2300 UTC, along a four-sided circuit. Velocity data were collected with a 1200 KHz Workhorse Acoustic Doppler Current Profiler (ADCP)

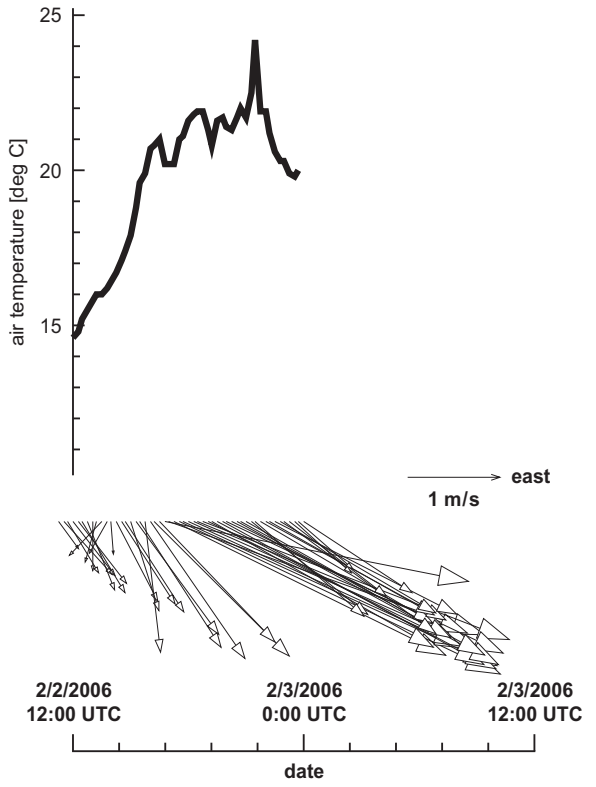

Fig. 2. Air temperature and wind direction time series for the Guana–Tolomato–Matanzas National Estuarine Research Reserve weather station, located approximately 30 km south of the study area, near the mouth of Pellicer Creek at 29°39.467 N, 81°13.217 W (NERRS, 2006).

mounted on a pole attached to the port side of a small (<5 m long) boat. Transducers were 0.3 m below the surface and pointed downward. The ADCP sampled 0.5 m bins in the vertical at 1 s intervals. Using ensemble average sets of 10 s, and cruising at an average speed of 1.5 m/s, the average horizontal resolution was 15 m. The bin located closest to the surface was at a depth of 1.5 m. The depth throughout the circuit was <16 m, which allowed operation of the ADCP in bottom tracking mode. Navigation was aided by a Global Positioning System (GPS) mounted directly above the ADCP, from which position and time were saved directly to a computer. These data were used to calibrate the ADCP compass, as in Joyce (1989).

Continuous surface hydrography (temperature and salinity) data were recorded with a Sea Bird SBE37 conductivity–temperature (CT) probe mounted astern. Data were stored in instrument memory every 10 s and synchronized with ADCP and GPS data after the survey. Vertical profiles of temperature and salinity were collected with a Sea Bird SBE19 conductivity–temperature-depth (CTD) recorder at seven locations shown in Fig. 1. Casts were performed every other circuit to cover the ends of the transect and its deepest part. Transect 1 was too shallow for a mid-transect cast. Thirteen repetitions of the underway sampling circuit were completed and 38 casts were made.

Data were organized onto uniform grids having a horizontal resolution of 15 m and a vertical resolution of 0.5 m. Each grid point had a time series of 13 values of east–west (u) and north–south (v) velocity components. A least-squares fit of the semidiurnal harmonic was applied to both the u and v velocities at each grid point. From this analysis, values of mean flow, amplitude, and phase for the semidiurnal constituent were obtained for the sampling period. These data were then used to reconstruct a velocity time series with

$$(u, v) = (\bar{u}, \bar{v}) + (u_{a1}, v_{a1}) \sin(\sigma_1 t + (u_{\theta_1}, v_{\theta_1})), \quad (2)$$

where $(\bar{u}, \bar{v})$ are mean flow, σ_1 is the M2 tidal frequency, and (u_{a1}, v_{a1}) and $(u_{\theta_1}, v_{\theta_1})$ are the semidiurnal velocity amplitude and phase components, respectively (e.g. Valle-Levinson et al., 2000b). Fig. 3 shows the least-squares fits of the reconstructed semidiurnal harmonic (Eq. (2)) for observed velocity components in the east–west and north–south directions at the mid-point of each transect, taken at a depth of 1.5 m. The fits are compared to the observed tide in Table 1. Goodness of fit parameters for each velocity component, averaged over depth and transect length, are presented in Table 2. On average, 86% of the total variability observed in the study area can be explained by Eq. (2). A simple time average of the observed velocities gives values similar to those obtained with the harmonic analysis of Eq. (2). At some shallow locations within the study area, Eq. (2) explains a lower percentage of the total variability due to limited data or through an excitation of over-tides near steep bathymetric gradients, which cause strong lateral shear (Hench and Luettich, 2003). When the M4 tidal harmonic is included in the analysis, 93% of the variability observed can be explained by the following equation:

$$(u, v) = (\bar{u}, \bar{v}) + (u_{a1}, v_{a1}) \sin(\sigma_1 t + (u_{\theta_1}, v_{\theta_1})) + (u_{a2}, v_{a2}) \sin(\sigma_2 t + (u_{\theta_2}, v_{\theta_2})), \quad (3)$$

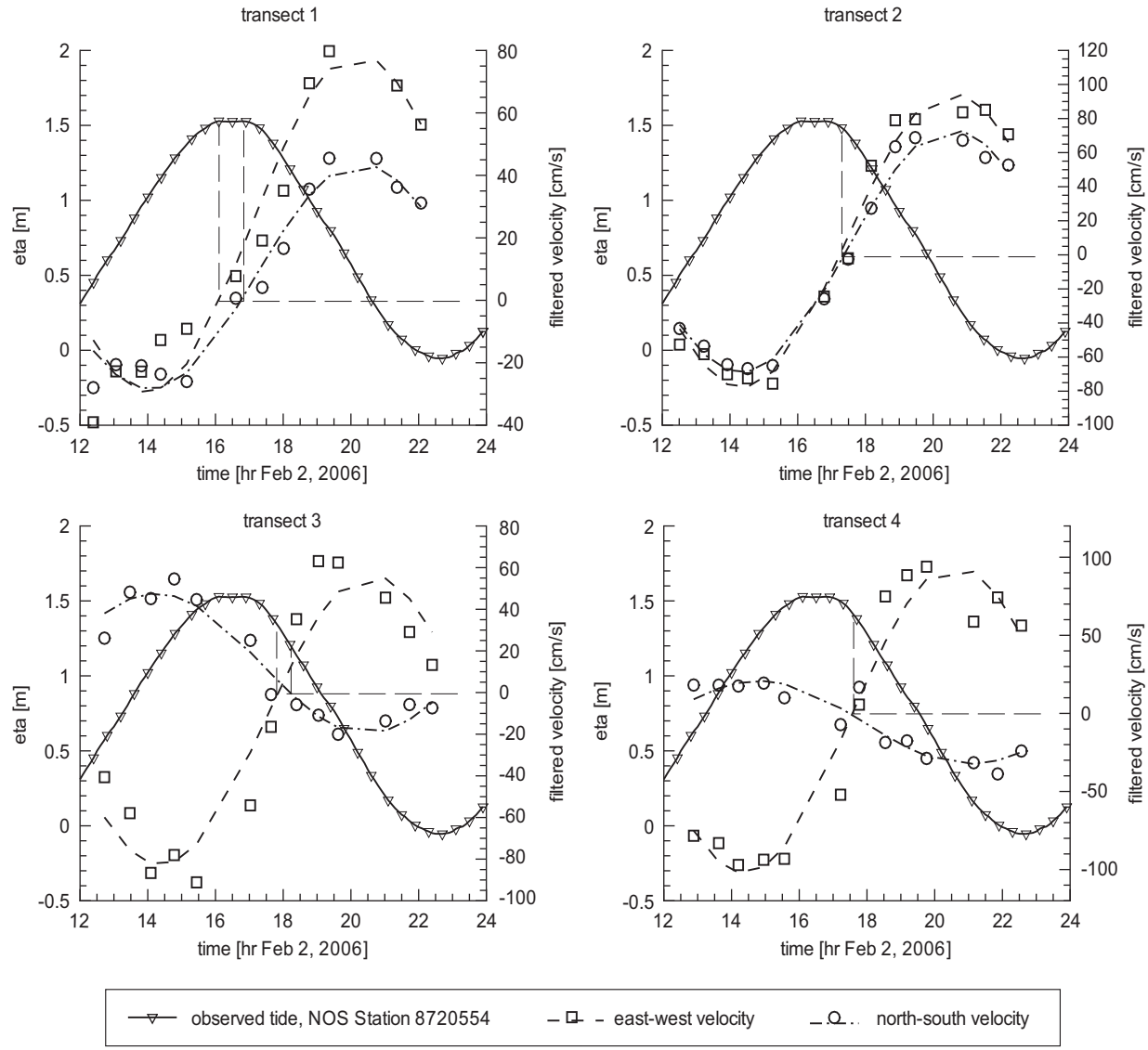

Fig. 3. Time series of observed tide at the National Oceanic and Atmospheric Administration's Ocean Service Station 8720554 (Vilano Beach Intra-coastal Waterway, Florida), as shown in Fig. 1; east–west and north–south near-surface velocity components at the midpoint of the four transects shown in Fig. 1. Short-dashed and dot-dashed lines are least-squares fit of the velocity to Eq. (2); symbols are observed data. Horizontal and vertical oriented long-dashed lines locate the tidal elevation that corresponds with the occurrence of zero velocity.

where σ_2 is the M4 tidal frequency, and (u_{a2}, v_{a2}) and $(u_{\theta_2}, v_{\theta_2})$ are the M4 velocity amplitude and phase components, respectively.

4. Results

This section details previously undocumented aspects at this location. These observations characterize the behavior of the system on the sampling date. Seasonal or shorter-term variations of these observations remain unexplored.

4.1. Observation of uniform surface hydrography and well-mixed conditions

Mean surface temperature, salinity, and density are shown in Fig. 4. The range of each variable is narrow. The locations of A–A′ and B–B′ are chosen to characterize the maximum gradient across the

Table 1
Goodness of fit parameters for the semidiurnal harmonic (Eq. (2)) least-squares fit of observed near-surface velocity, at the midpoints of the four transects shown in Fig. 1. Observed and fit velocity are shown in Fig. 3; e–w is east–west velocity component; n–s is north–south velocity component

Transect	Goodness of fit		Root mean square error (cm/s)	
	e–w	n–s	e–w	n–s
1	0.927	0.963	11.67	5.15
2	0.984	0.989	8.38	7.06
3	0.91	0.948	16.54	5.79
4	0.951	0.863	19.72	8.73

Table 2
Goodness of fit and root mean square error values averaged over depth and distance for each transect; e–w is east–west velocity component; n–s is north–south velocity component

Transect	Goodness of fit		Root mean square error (cm/s)	
	e–w	n–s	e–w	n–s
1	0.844	0.843	12.6	8.87
2	0.945	0.936	9.77	8.14
3	0.87	0.805	14.43	8.83
4	0.911	0.761	15.9	9.22

narrow dimension of the domain. These gradients are not always small: the A–A′ temperature gradient and A–A′ density gradient are five and 15 times larger than the gradient across the B–B′ dimension. While the larger gradients associated with lobes of mean hydrography are not small, they are localized, or confined to a small region within the study domain. Fig. 4 shows that the majority of the study domain falls within a mean surface density range of 24.66 and 24.68 kg/m^3, and that the low density lobe is localized.

The instantaneous vertical density distribution is shown throughout the sample period at six cast locations in Fig. 5. An absence of vertical structure in the density field of Fig. 5 suggests a lack of stratification during the sampling period. Let the baroclinic pressure gradient be approximated as

$$\frac{1}{\rho_0}\frac{\Delta\rho}{\Delta x}\,gH, \tag{4}$$

where ρ_0 is representative density, and $\Delta\rho/\Delta x$ is the instantaneous density gradient in some horizontal direction x. Using representative density values from Fig. 4, and representative depth values from Fig. 1, the baroclinic pressure gradient between A–A′, B–B′, and C–C′ of Fig. 4 is $5.4\times10^{-6}\,m/s^2$, $-7.5\times10^{-7}\,m/s^2$, and $1.1\times10^{-6}\,m/s^2$. As shown in Section 5, relative to other forcing mechanisms, the baroclinic pressure gradient is weak. The domain is therefore characterized as well mixed during the sampling period.

4.2. Fronts aligned with bathymetry

Numerous investigators have addressed the formation of axial convergence fronts in well-mixed and partially mixed estuaries (i.e. Nunes and Simpson, 1985; Li, 2002). These fronts may be driven by lateral shears of along-estuary flows that develop in regions where bathymetry changes rapidly. Convergence fronts and regions of flow divergence in well-mixed estuaries may be characterized by changes in tidal current ellipticity—the ratio of the major to minor axes—of adjacent tidal ellipses; and changes in the orientation of the major axes of adjacent tidal ellipses. Sharp changes in surface roughness—evidence of a convergence front—were observed during ebb near the intersection of Transects 1 and 4. The ellipticity and the tilt of the major axis change rapidly in this region (Fig. 6). This is also a region of strong bathymetric gradient (Fig. 1).

Surface velocity and surface salinity, plotted in the time-latitude domain across Transect 4, are shown in Fig. 7. The orientation of surface velocity vectors show that flow across Transect 4 is clearly divergent during flood, before Hour 16.5; and convergent during ebb, after Hour 17.5. Valle-Levinson et al. (2000a) show that convergence fronts form during both ebb and flood in the James River Estuary, Virginia, USA, generated by the interaction of tide with bathymetry and the density field. A similar causal relationship may exist at St. Augustine Inlet. Examination of three points in the time-latitude domain (Fig. 7) shows that areas of flow divergence or convergence (between J and J′ and L and L′) generate salinity gradients that are one order of magnitude higher than areas of the domain that do not exhibit flow convergence or divergence (between K and K′). Sharp salinity gradients are a surrogate for sharp density gradients, here, where salinity served as a better proxy for density than temperature during the sampling period. Point pairs J and L are also in an area of the time-latitude domain with steep bathymetric gradients (Fig. 1) and tidal extrema, while Point pair

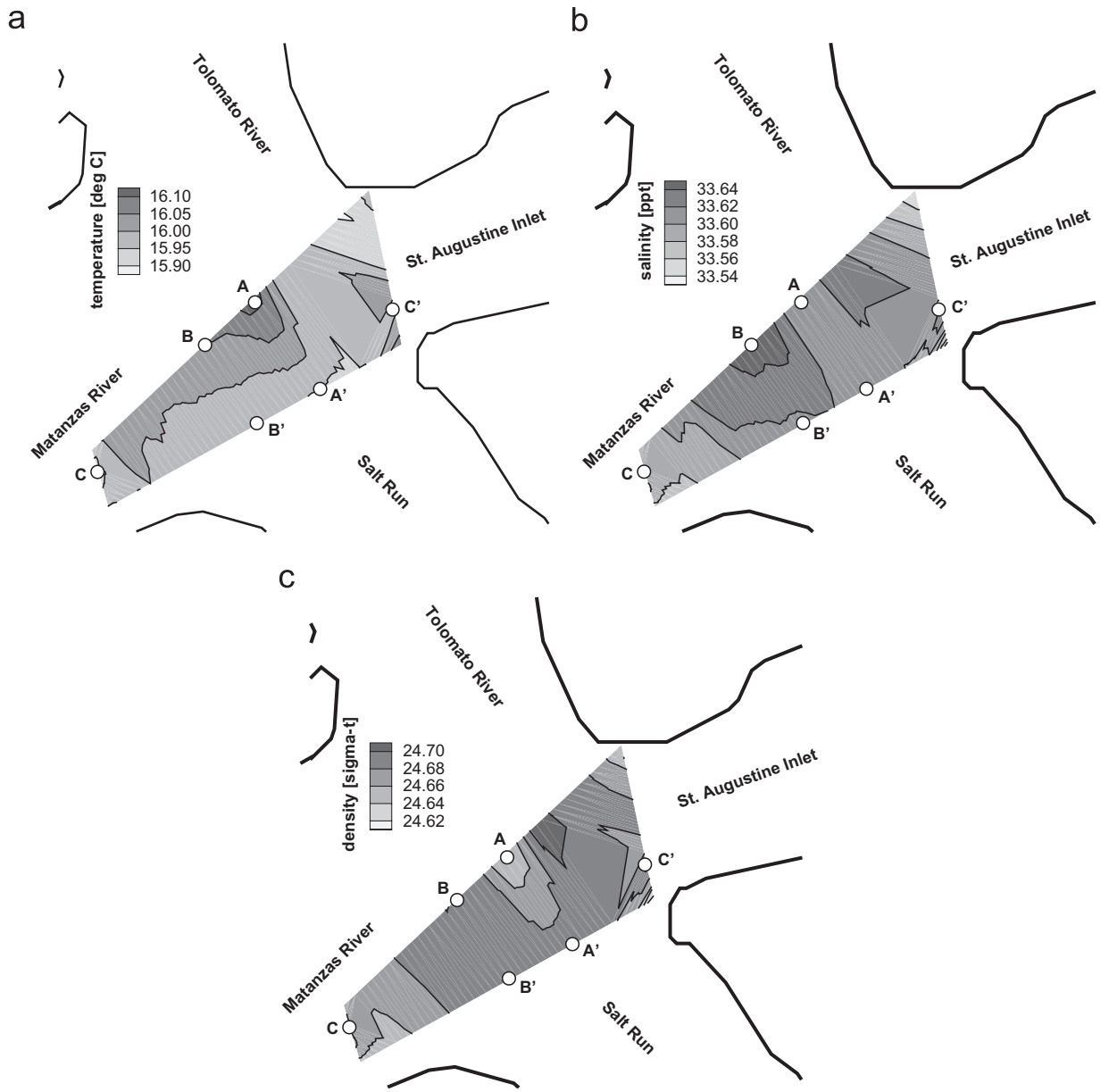

Fig. 4. Mean surface (a) temperature, (b) salinity, and (c) density between Julian Day 33.53 and 33.91, 2006. Horizontal mean surface gradients in the A–A, B–B, and C–C′ directions are -3.9×10^{-4} °C/m, -8.1×10^{-5} °C/m, and 7.4×10^{-5} °C/m for mean surface temperature; 2.2×10^{-5} psu/m, -3.3×10^{-5} psu/m, and 5.9×10^{-5} psu/m for mean surface salinity; and 1.1×10^{-4} kg/m^4, -6.8×10^{-6} kg/m^4, and 2.8×10^{-5} kg/m^4 for mean surface density.

K is in an area of shallow bathymetric gradient (Fig. 1) at slack tide. Note that both ellipticity and orientation gradients of surface tidal ellipses in Fig. 6 reinforce the idea that this is a region of divergence during flood and convergence during ebb. An additional region of ebb-flow convergence and flood-flow divergence occurred near the mid-point of Transect 3, as shown by orientation gradients in Fig. 6.

4.3. Observation of low-salinity environment offshore

Ebb flows across Transect 4 are less saline than flood flows; surface flow and salinity are therefore

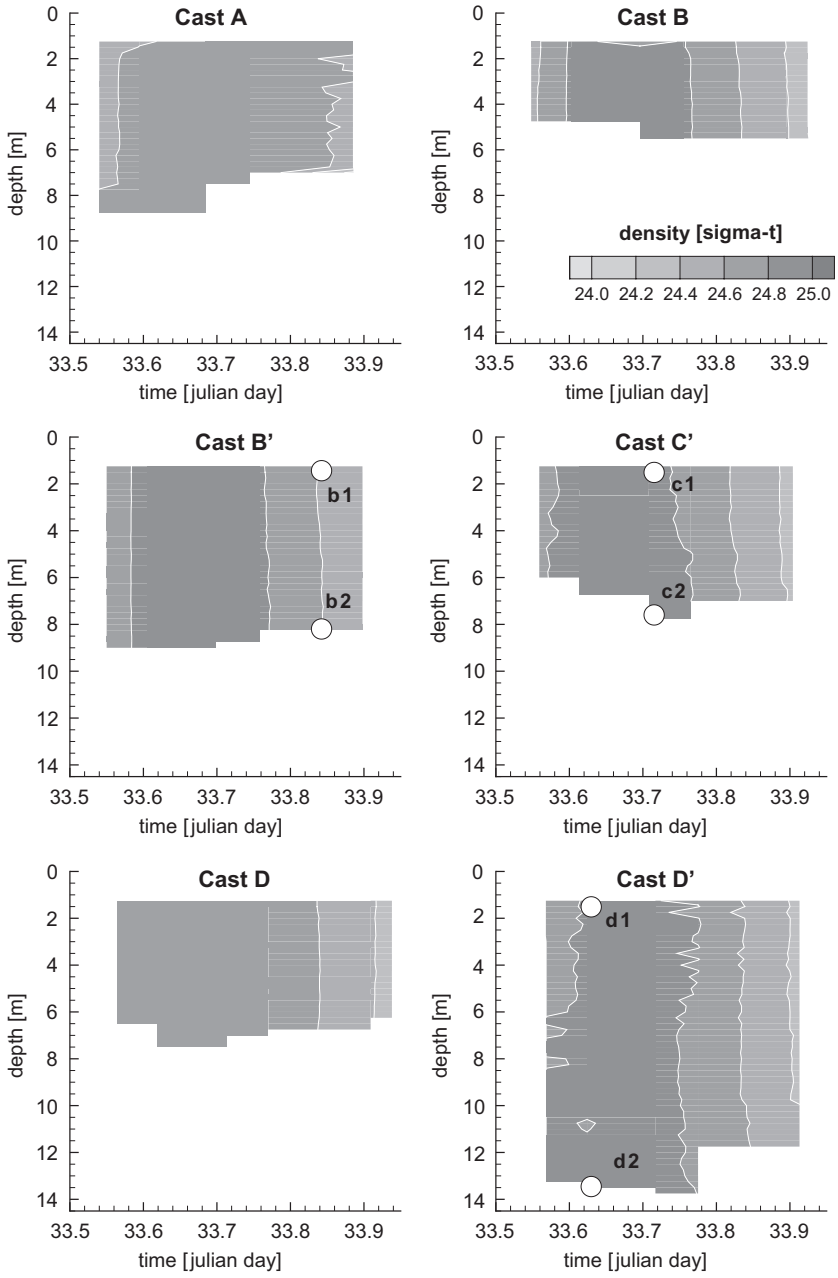

Fig. 5. Vertical density gradient as a function of depth and time at six cast locations. Instantaneous vertical density gradients between points b1 and b2, c1 and c2, and d1 and d2 are 3.1×10^{-3} kg/m^4, 4.2×10^{-3} kg/m^4, and 1.8×10^{-3} kg/m^4.

covariant across Transect 4 (Fig. 7). Note that flood flows are of a salinity less than 34; higher than the salinity inside the inlet but less than typical oceanic salinity of 35. Blanton and Atkinson (1983) and Atkinson et al. (1983) suggest that during the winter, freshwater input to the inner shelf of the South Atlantic Bight creates a low-salinity coastal environment in this area. Freshwater is supplied through the estuarine systems of South Carolina, Georgia, and North Florida. Flood flows to the Guana–Tolomato–Matanzas Estuary are a combination of ocean water and freshwater sources to the north. Because salinity might be considered a tracer for transported matter, such as pollutants or larvae, one implication for this observation is the existence of some inter-estuarine communication. Some fresh

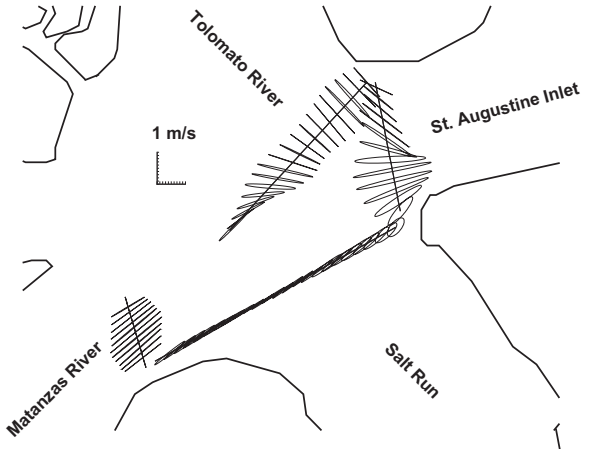

Fig. 6. Surface tidal ellipses constructed from the semidiurnal velocity amplitude and phase (Eq. (2)).

water discharged to Atlantic shelf waters, from systems to the north, is transported into the Guana–Tolomato–Matanzas Estuary.

4.4. Relationship between sea level and tidal flow

The semidiurnal phase for flow and sea level, and the velocity–tide phase lags are detailed in Table 3. A quasi-standing wave behavior is qualitatively evident in Fig. 3 as the point of zero velocity approximately corresponds with the tidal extrema. The time series are approximately 90° out of phase. The tide station is located approximately 1300 m north of the centroid of the study domain. It is an assumption of this analysis that water-surface elevation at the tide station is representative of the entire domain, and that the time series at the tide station is representative of the time series at the midpoint of each transect, with no time lag. (While this is strictly not the case, this assumption does not alter the conclusion that a quasi-standing wave existed in the study domain. Note that a shallow water wave in 5 m of water will travel 1300 m in approximately 3 min. The time lag from the tide station to the study domain is insignificant for the purposes of this analysis.) On the basis of the tidal properties in the study area, the tidal residual flow should be similar to that predicted by Li and O'Donnell (2005) for short channels: net inflow in the channel and net outflow over the shoals.

4.5. Mean flow patterns

Mean near-surface and near-bottom velocities are shown in Fig. 8. The flow direction is relatively uniform in the vertical: an attribute of a well-mixed estuary. Note a large counter-clockwise recirculation in the center of the domain, at both the surface and bottom. Also apparent are a small clockwise gyre in the northeast corner of the domain at the surface and bottom, and a small clockwise recirculatory gyre on the west side of the domain at the bottom. These gyres govern intra-estuarine communication, by either enhancing or hindering the transport of materials between tributaries. Changes in the structure of the recirculation may impact the efficiency of this communication. The presence of these gyres also affects the efficiency of inter-estuary communication, governing the distribution of oceanic constituents—sourced from other estuaries—within the Guana–Tolomato–Matanzas Estuary. For instance, Churchill et al. (1999) showed that residual circulation at Beaufort Inlet, North Carolina caused biotic zonation in the estuary.

Mean velocities, oriented approximately perpendicular to Transects 2–4, are shown in Fig. 9. For Transect 4, mean outflow occurred over the shoals while mean inflow was found in the channel. Similar to Transect 4, mean outflow developed over the shoals and mean inflow in the channel, across the Tolomato River at Transect 3. The opposite flow pattern occurred at Transect 2 across the Matanzas River: mean outflow in the channel and a weak mean inflow over the southern shoal, near the bed. The weak mean flow perpendicular to Transect 1 indicates that Salt Run is a weakly flushed tributary.

Stommel and Farmer's (1952) source–sink analog is a viable explanation for the observation of mean flow at Transect 4. Chadwick and Largier (1999) showed that the superposition of source and sink flow at the entrance to San Diego Bay gives rise to lateral variations in the subtidal flow similar in character, but opposite in direction, to that observed at Transect 4 (Fig. 9). The mean flow observed at Transect 4 is also similar to Li and O'Donnell's (2005) theoretical model of mean flow in a short channel.

5. Discussion

Dominant forcing mechanisms in the study area are determined here by considering the relative contributions of advective and Coriolis accelerations, bottom friction, and the baroclinic pressure gradient. This is done by first applying a scaling analysis to the x- and y-momentum equations, and then through a relative magnitude analysis. Light winds during the study period eliminate wind stress as a dominant

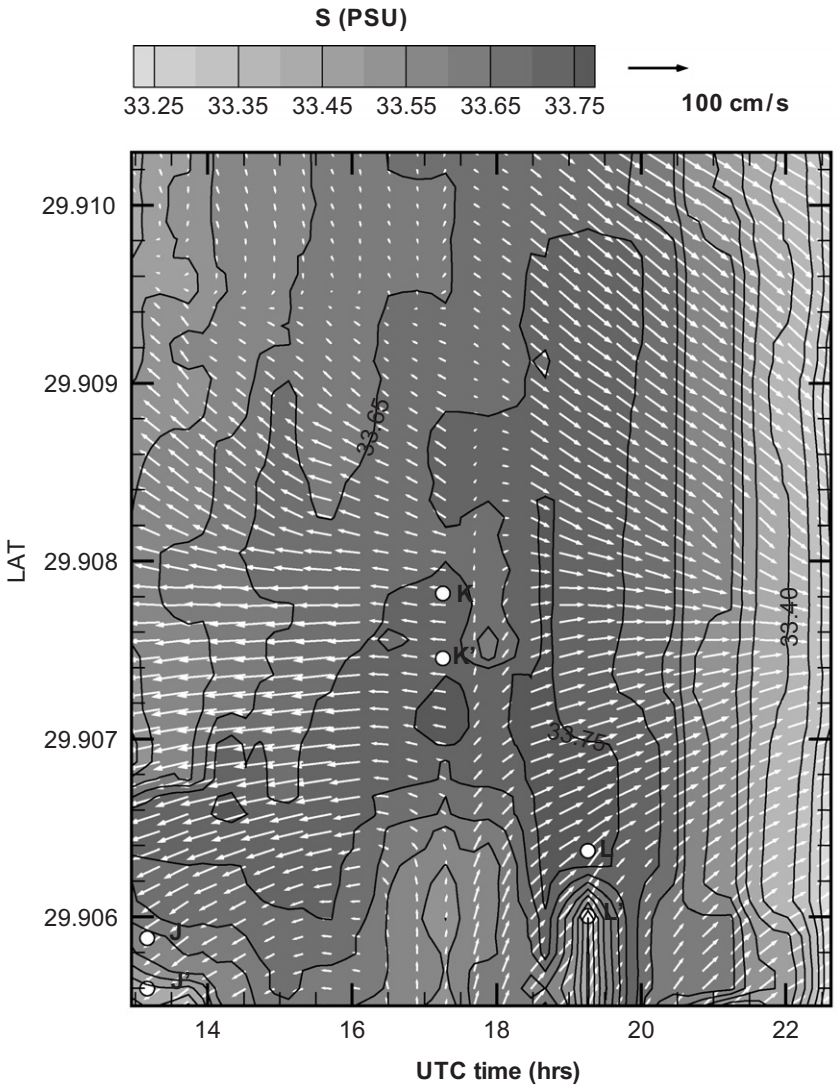

Fig. 7. Surface salinity and velocity as a function of time and latitude, across Transect 4. Flood flows are drawn with vectors that point to the left. Instantaneous surface density gradients between Points J and J′, K and K′, and L and L′ are -4.34×10^{-3}, 4.13×10^{-4}, and -6.94×10^{-3} ppt/m. The J and L gradients are in areas within the time-latitude domain that exhibit flow divergence and convergence. The K gradient is in an area of the time-latitude domain that does not exhibit flow divergence or convergence.

Table 3
Velocity and tide phase, and velocity–tide phase lag, at the midpoints of the four transects shown in Fig. 1; e–w is east–west velocity component; n–s is north–south velocity component

Transect	Phase				
	Velocity		Tide	Velocity–tide phase lag	
	e–w	n–s		e–w	n–s
1	45	42	−26	70	68
2	34	34	−26	60	60
3	33	37	−26	59	63
4	33	21	−26	59	46

forcing mechanism: tidal advective accelerations were typically $O(10^{-4})\,\mathrm{m/s^2}$, whereas accelerations produced by wind stress at the inlet were $O(10^{-6})\,\mathrm{m/s^2}$.

5.1. Scaling analysis

In a right-handed coordinate system, where x is aligned with the streamwise direction and is positive seaward, the tidally averaged momentum equations may be scaled to determine the dominant dynamics. The equations used in the following scaling analysis are given by Eqs. (5) and (6). Horizontal friction

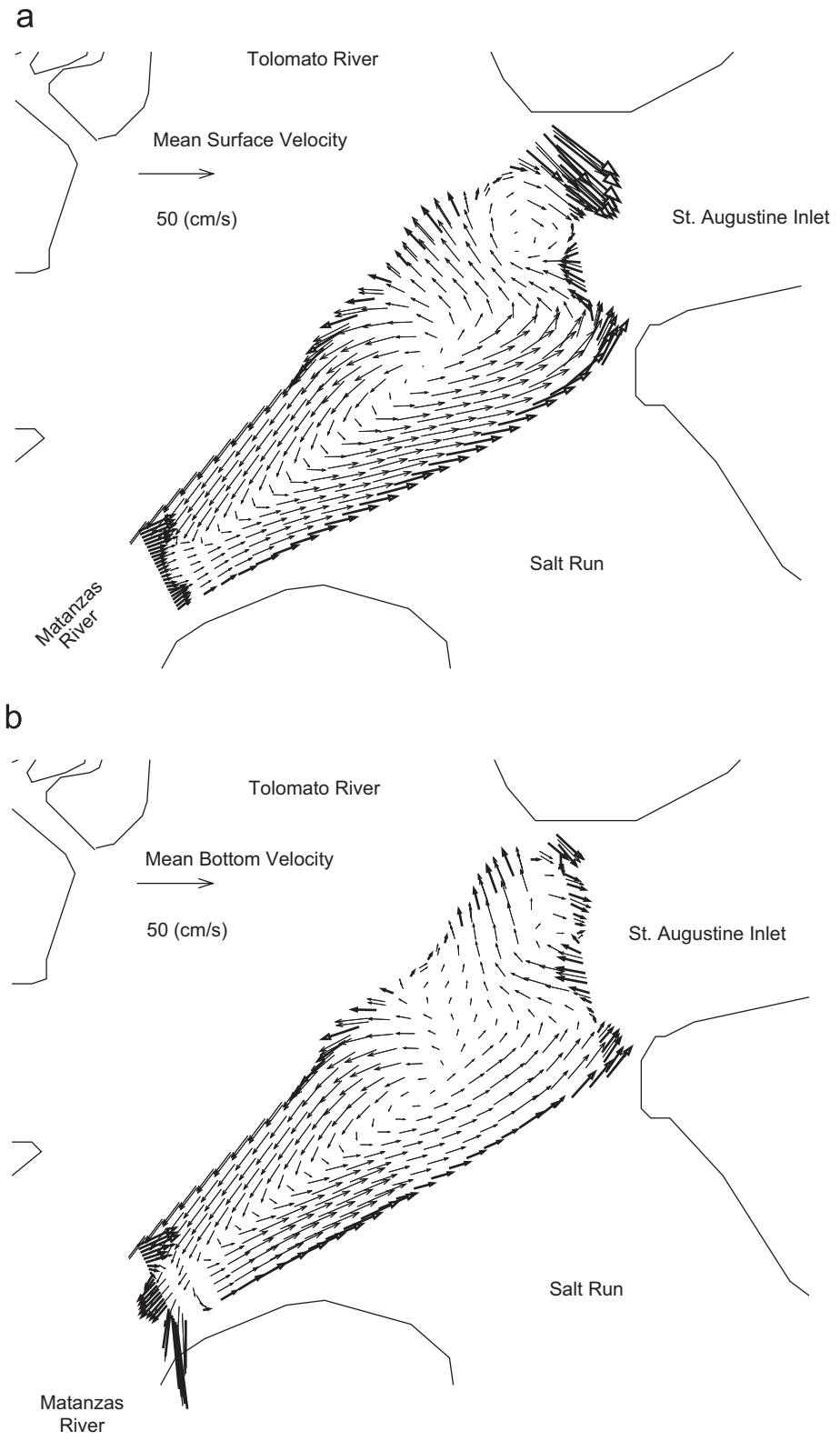

Fig. 8. Mean (a) surface and (b) bottom velocities between Julian Day 33.53 and 33.91, 2006. Bold-lined vectors located around the edge of the study domain were generated with the reconstructed semidiurnal velocity components. Thin-lined vectors located in the interior of the domain were generated by interpolation of the bold-lined vectors using an inverse distance method.

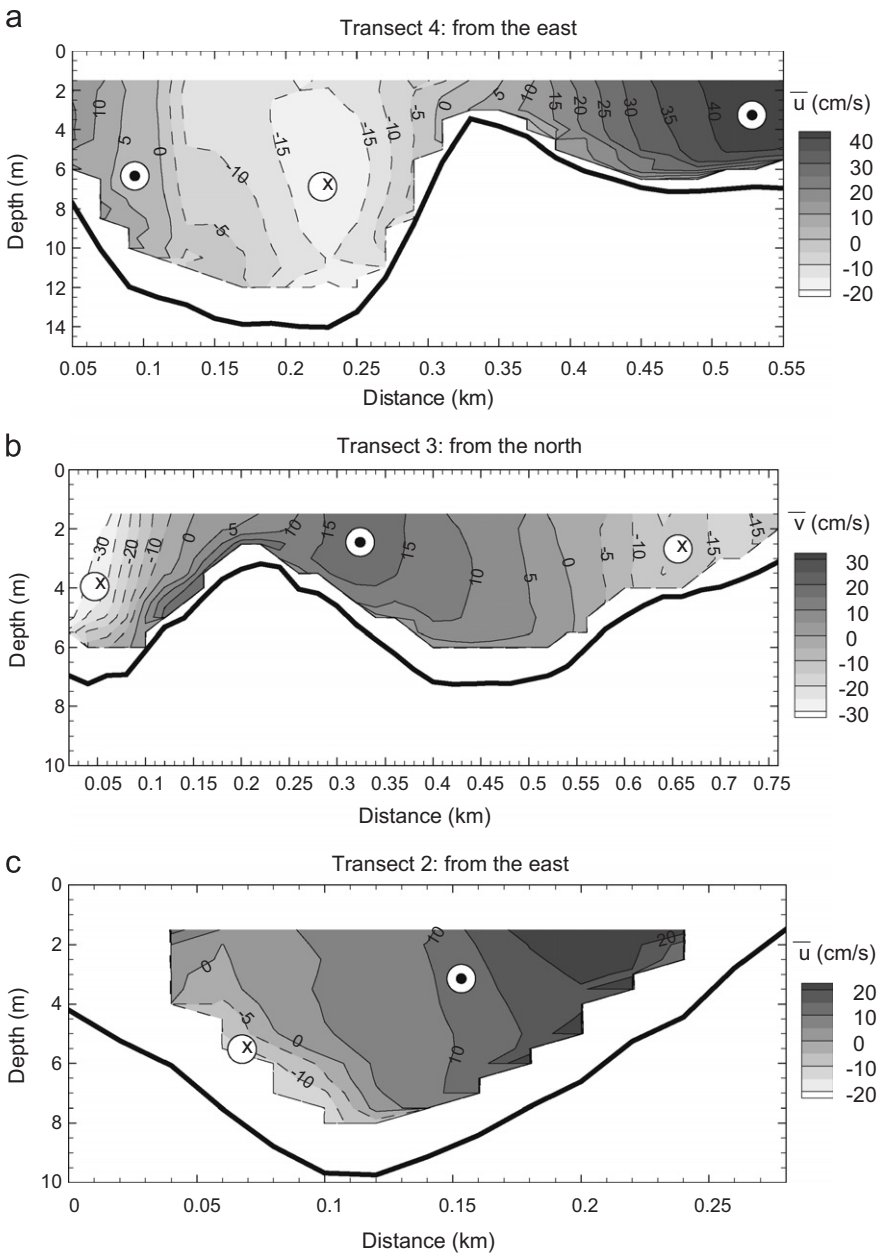

Fig. 9. Mean velocity across (a) Transect 4, at the inlet; (b) Transect 3, at the mouth of the Tolomato River; and (c) Transect 2, at the mouth of the Matanzas River. u velocity is east–west; v velocity is north–south. Circles with dots denote regions of flow out of the figure; circles with the letter x denote regions of flow into the figure. Solid line velocity contours are $\geqslant 0$; dashed line velocity contours are <0. A lateral u-velocity gradient of $2.0 \times 10^{-3}\,\mathrm{s}^{-1}$ existed across Transect 4, between the north shoal and the center of the channel. A similar magnitude channel-to-shoal, v-velocity gradient of $1.8 \times 10^{-3}\,\mathrm{s}^{-1}$ existed at Transect 3.

terms are neglected in this analysis.

$$\left\langle u\frac{\partial u}{\partial x}\right\rangle + \left\langle v\frac{\partial u}{\partial y}\right\rangle + \left\langle w\frac{\partial u}{\partial z}\right\rangle - \langle fv\rangle = -\left\langle \frac{1}{\rho_o}\frac{\partial p}{\partial x}\right\rangle + \left\langle \frac{\partial}{\partial z}\left(A_v\frac{\partial u}{\partial z}\right)\right\rangle, \quad (5)$$

$$\left\langle u\frac{\partial v}{\partial x}\right\rangle + \left\langle v\frac{\partial v}{\partial y}\right\rangle + \left\langle w\frac{\partial v}{\partial z}\right\rangle + \langle fu\rangle = -\left\langle \frac{1}{\rho_o}\frac{\partial p}{\partial y}\right\rangle + \left\langle \frac{\partial}{\partial z}\left(A_v\frac{\partial v}{\partial z}\right)\right\rangle, \quad (6)$$

where f is the Coriolis parameter, p is pressure, A_v is vertical eddy viscosity, and $\langle\ \rangle$ is a time-averaging operator. Representative velocity (U, V), length (L_x, L_y), and depth (H) scales for the system are $U\sim0.2\,\mathrm{m/s}$, $V\sim0.1\,\mathrm{m/s}$, $L_x\sim750\,\mathrm{m}$, $L_y\sim450\,\mathrm{m}$, and $H\sim7.5\,\mathrm{m}$. The scaling analysis, presented in Table 4, demonstrates that advective terms are approximately five times larger than both friction and Coriolis, and that the contribution of the baroclinic pressure gradient to the subtidal momentum balance is small compared to other terms. Results of this analysis suggest that the subtidal dynamics of the system are described by a balance between advective acceleration and the barotropic pressure gradient, or what others have referred to as Bernoulli-type dynamics (i.e. Ott and Garrett, 1998; Valle-Levinson et al., 2000b). The barotropic pressure gradient is the driving force for the flow in this system.

Because the values of U and V are similar, a scaling analysis for Eq. (6) yields values close to those given in Table 4. Although a representative vertical velocity for this system is unknown, it is assumed that w is small compared to U and V; therefore, terms of w are excluded. In order to determine the relative contributions of advective acceleration, Coriolis acceleration, and bottom friction to the mean momentum balance, their relative magnitudes are compared in the following sections.

5.2. Advective versus Coriolis accelerations

The relative magnitude of advective acceleration to Coriolis acceleration is plotted in Fig. 10 for Transects 1–4. Advective accelerations are typically one order of magnitude larger than Coriolis accelerations. The transect across Salt Run (Figs. 10(a) and (b)) shows localized regions where Coriolis may be important, but these areas are small compared to the remaining area of the transect, which is dominated by friction. Areas dominated by advective processes tend to correspond with areas of steep bathymetric gradients, where flow convergence and divergence give rise to strong longitudinal and lateral shears. The uniform bathymetry over most of Transect 1 may account for the decreased influence of advective accelerations.

Table 4
Scaling analysis of Eq. (5). The canonical form of the drag coefficient is adopted, where $C_d = 0.0025$. The local value of f is taken as $f = 7\times10^{-5}\,\mathrm{s^{-1}}$. The representative density gradient is $\partial\rho/\partial x = 2\times10^{-5}\,\mathrm{kg/m^3/m}$, and the reference density is $\rho_o = 1024.675\,\mathrm{kg/m^3}$

Term	Scaled term	Value ($\times10^{-5}\,\mathrm{m/s^2}$)
$\left\langle u\frac{\partial u}{\partial x}\right\rangle$	UU/L_x	5
$\left\langle v\frac{\partial u}{\partial y}\right\rangle$	VU/L_y	4
$\langle fv\rangle$	fV	1
$\left\langle\frac{\partial}{\partial z}\left(A_v\frac{\partial u}{\partial z}\right)\right\rangle$	C_dUU/H	1
$\left\langle\frac{g}{\rho_0}\int\frac{\partial\rho}{\partial z}\mathrm{d}z\right\rangle$	$\frac{1}{\rho_0}\frac{\partial\rho}{\partial x}gH$	0.1

5.3. Advective acceleration versus bottom friction

The effects of bottom friction throughout the system are studied using a parameterization of vertical eddy diffusivity $A_v\,\partial u/\partial z = C_d u|\vec{v}|$, where C_d has the canonical value of 0.0025 (Rivière et al., 2004). To aid in the comparison of terms, it is assumed here that dissipation occurs over the entire water column. Again, with the exception of Salt Run, advective accelerations are often one order of magnitude greater than bottom friction (Fig. 11). In some localized regions, bottom friction dominates the comparison (Figs. 11(f) and (g)). These areas are likely characterized by strong vertical shears. However, there appear to be more areas dominated by advective acceleration than by bottom friction throughout Transects 2–4. Transect 1 (Figs. 11(a) and (b)) shows a more widespread dependence on bottom friction than other transects. This may be attributed to comparatively shallow bathymetry, the fact that mean flow is in the along-transect direction, and that mean-flow magnitude does not vary significantly in space.

5.4. Bottom friction versus Coriolis acceleration

The dominant term in this comparison is less obvious than in the previous two ratios, as demonstrated in Fig. 12. The stream-normal balance at the mouth of Salt Run appears to be dominated by bottom friction while the streamwise component demonstrates a larger dependence on Coriolis (Figs. 12(a) and (b), respectively). This discrepancy can be attributed to the stronger u velocity along this transect and the comparatively weak v velocity in the streamwise direction. Another example of this behavior is illustrated in Figs. 12(g) and (h) across

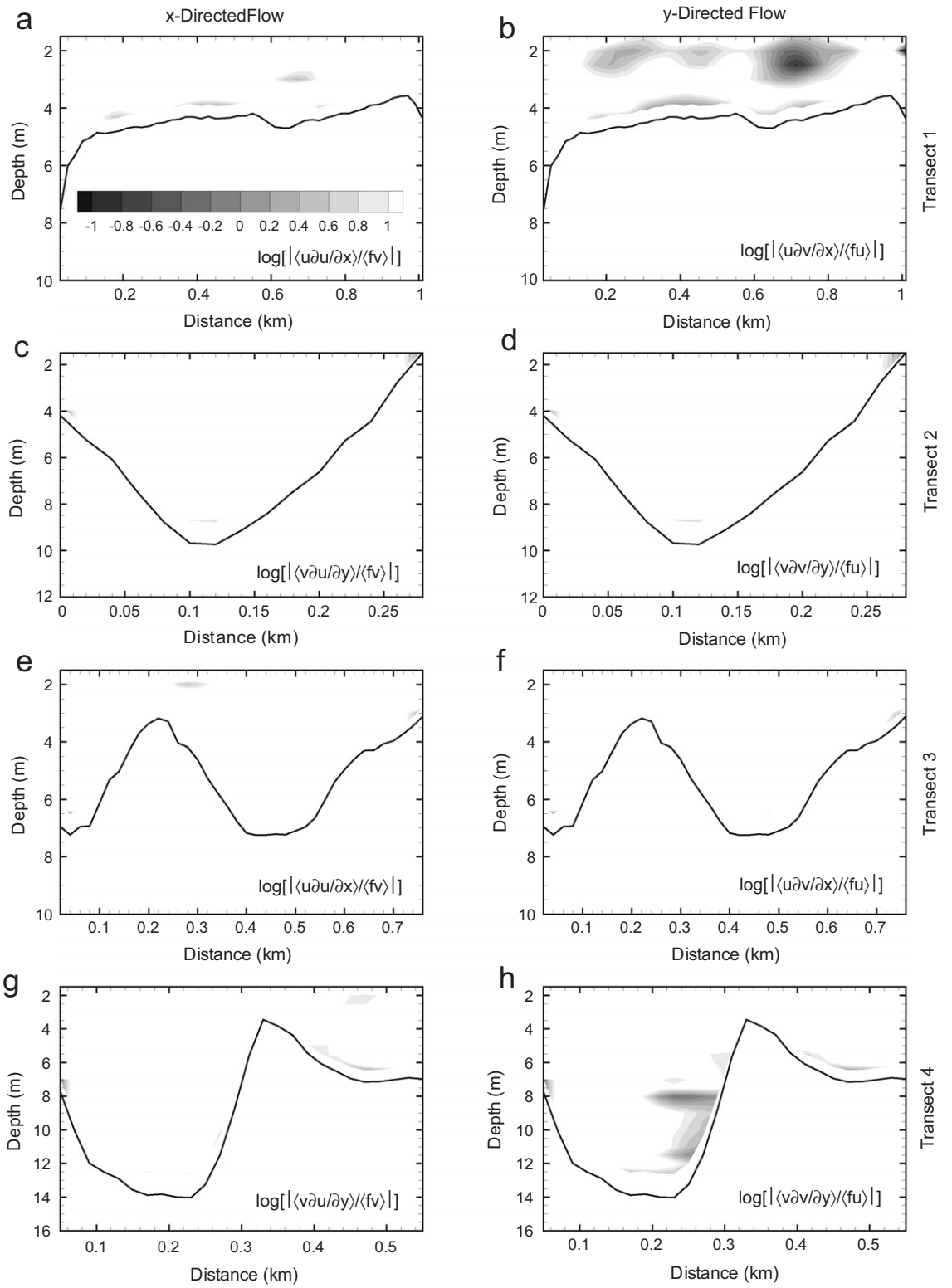

Fig. 10. Relative magnitudes of advective acceleration to Coriolis acceleration for Transects 1–4. Panels (a) and (b) show Transect 1 as viewed by an observer looking southward. Panels (c) and (d) show Transect 2 as viewed by an observer looking westward. Panels (e) and (f) represent Transect 3 as viewed by an observer looking southward. Panels (g) and (h) show Transect 4 as viewed by an observer looking westward. Only 90% of the data between the surface and bed are plotted; the remaining 10% of the data are not plotted due to side-lobe effects near the bed. Areas dominated by advection are represented by areas of light gray to white.

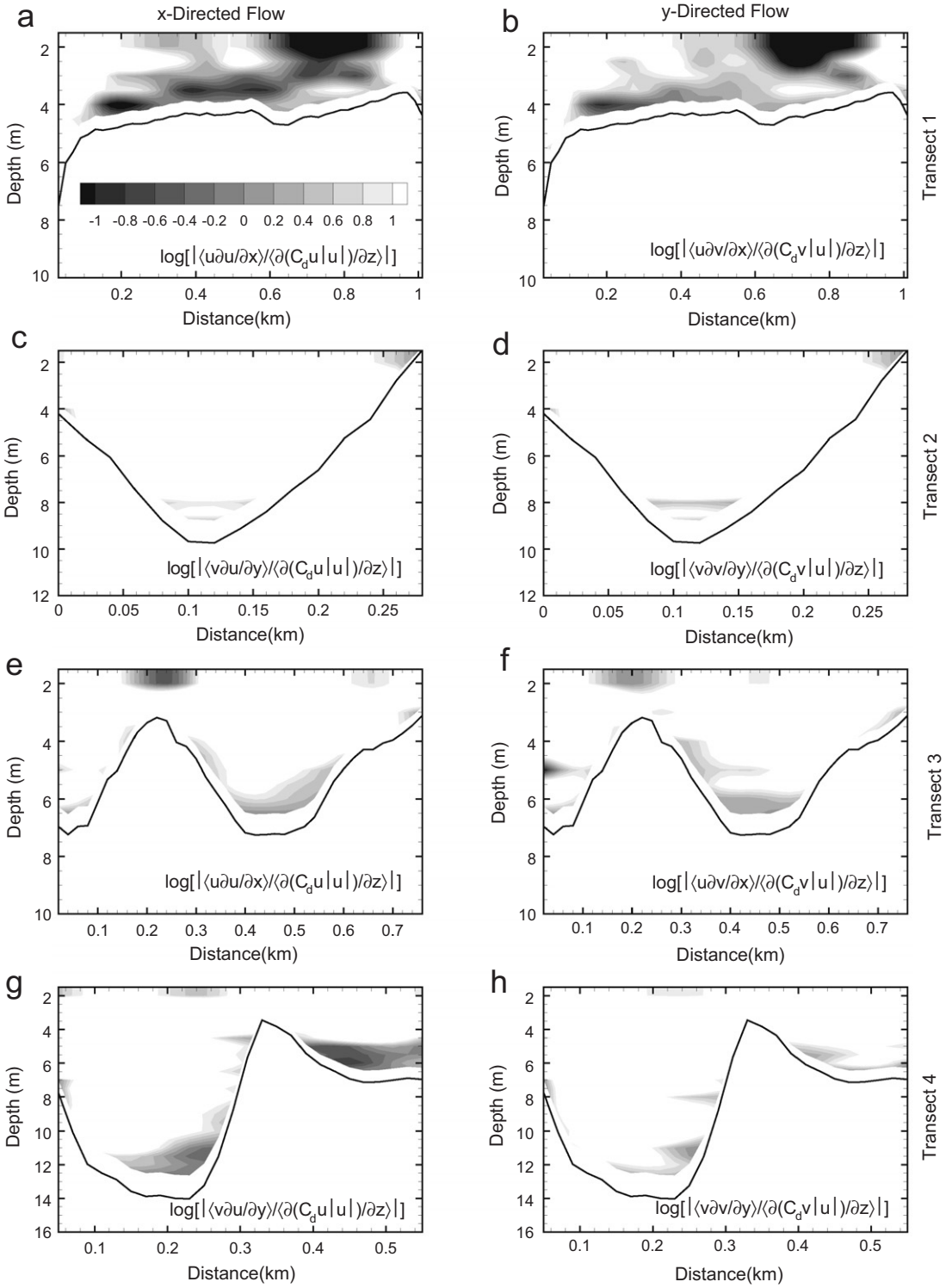

Fig. 11. Relative magnitudes of advective acceleration and bottom friction in Transects 1–4. The plotting convention is similar to that of Fig. 10. Areas dominated by advection are represented by areas of light gray to white.

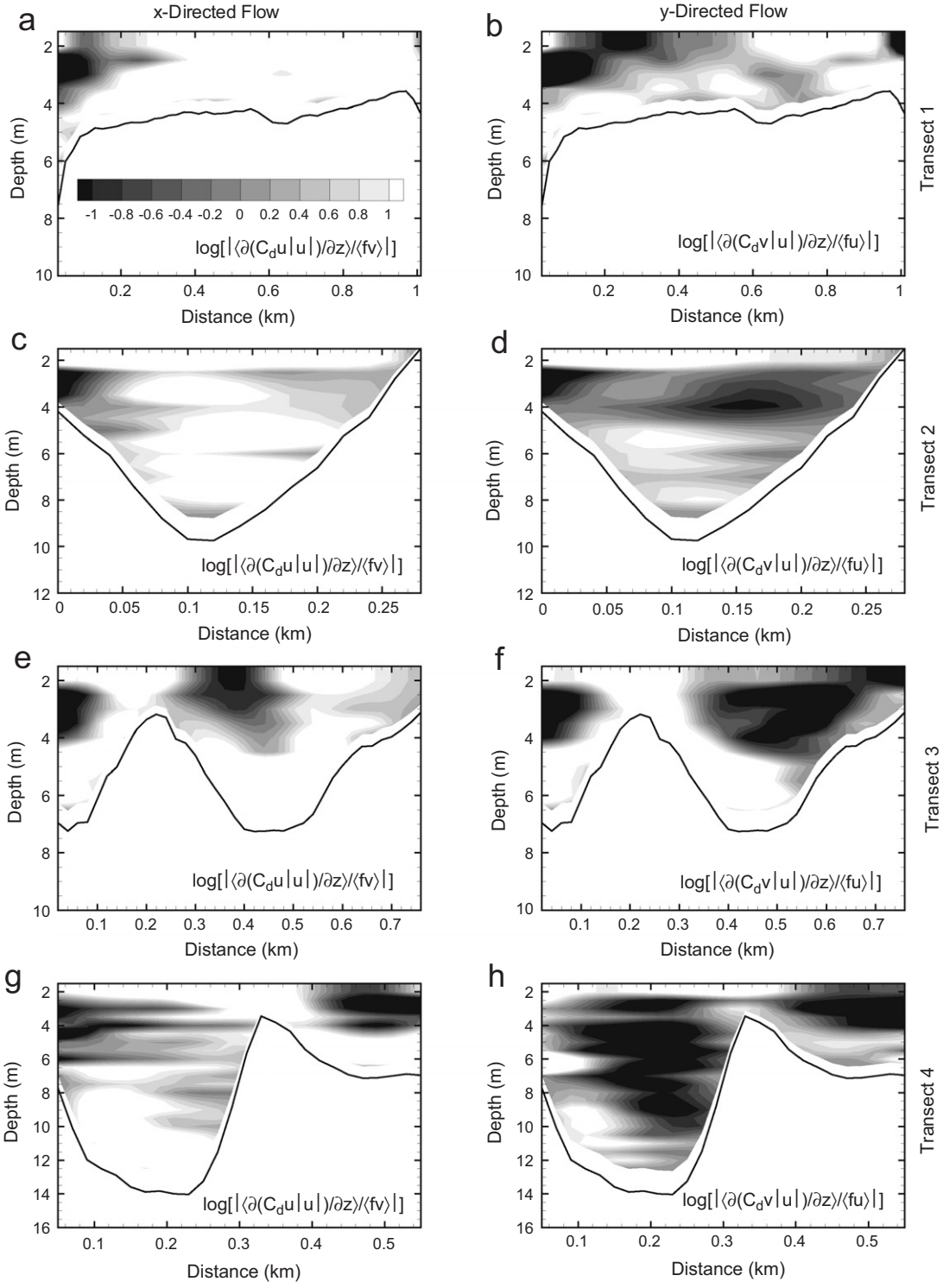

Fig. 12. Relative magnitude of bottom friction to Coriolis acceleration for Transects 1–4. The plotting convention is similar to that of Fig. 10. Areas dominated by friction are represented by areas of light gray to white.

the mouth of St. Augustine Inlet, where the mean flow is oriented in the east–west direction. The weak v velocity in the inlet causes values of bottom friction in the stream-normal direction to be small compared to values of the Coriolis acceleration. While the dominant term in the ratio between bottom friction and Coriolis may be difficult to determine from Fig. 12, the contribution of bottom friction is many times larger than that of the Coriolis acceleration, as determined by summing the contributions of each process over the entire transect and comparing their scaled magnitudes. This analysis is addressed in the following section.

5.5. System dynamics

Summing the contributions of the magnitudes of the various terms—advective acceleration, Coriolis acceleration, and bottom friction—over each transect, and then scaling them by the contribution of Coriolis for that transect, offers a quantitative comparison of their relative importance. These data are presented in Table 5. The analysis, along with Figs. 10–12, suggest that advection is a more dominant component of the momentum balance than either friction or Coriolis. This is especially true in regions with sharp bathymetric gradients. The contribution of friction to the system appears to be less widespread than advection, but it should not be completely neglected as an important dynamical process in localized regions of the system. This is demonstrated by the contribution of friction in areas of relatively low advective acceleration. Perhaps not surprising due to the small spatial scales associated with the system (<1 km), Coriolis does not appear to have a significant effect on the residual circulation. Although some of the transects, such as Transect 4 (Fig. 12), suggest that friction is less important than Coriolis in the transverse balance, there is typically so much shear that advection dominates the momentum balance.

Table 5
Order of magnitude analysis. Values are $\times 10^{-4}$ m/s^2

Transect	1	2	3	4
Term	Salt Run	Matanzas River	Tolomato River	St. Augustine Inlet
Advection	15	14	14	9
Friction	6	3	6	4
Coriolis	1	1	1	1
Baroclinicity	$\ll 1$	$\ll 1$	$\ll 1$	$\ll 1$

According to Li and O'Donnell's (2005) model, the system studied can be characterized as a "short channel." Their model requires that the system be closed at the head. Adopting the full 3.75 km length of Salt Run as the shortest pathway through the study area to a closed boundary, and a 4 to 7 m representative depth between Transect 4 and 1, a representative range of the dimensionless channel length parameter for St. Augustine Inlet is $0.4<\delta<0.56$. This range corresponds with a short channel, accurately characterized by the observed standing tidal wave. Their theory, however, should not be considered the only explanation for the residual circulation across Transect 4. The assumed system is not actually closed: flow also enters and exits this system through the Matanzas and Tolomato Rivers. Additionally, no attempt is made here to distinguish between the effects of tidal forcing from both inlets in the system. The source–sink analog of Stommel and Farmer (1952) might also be used to explain the residual circulation pattern across Transect 4. During ebb, stronger converging flows leave the estuary over the shoals. Assuming an insignificant freshwater input, weaker diverging flows exist in the shoal regions during flood. Averaging stronger ebb and weaker flood flows over the shoal region produce net outflow over the shoals, while strong advection in the system promotes mean inflow through the channel.

6. Inter-comparison of inlet-proximate split-flows

The residual circulation patterns observed at St. Augustine Inlet during the study period are consistent with, but perhaps not fully explained by both the Li and O'Donnell (2005) model of tidally induced residual flows and the source–sink analog of Stommel and Farmer (1952). Existing literature contains three well-documented studies of residual circulation patterns at inlet-proximate tidally driven splits. The characteristics and subtidal properties of the three systems listed in Section 1 are compared to the St. Augustine Inlet split to elucidate commonalities between forcing mechanisms and residual circulation patterns (Table 6). Where not directly stated in the literature, governing forcing mechanisms selected in Table 6 were hypothesized by considering system characteristics and the resulting mean flow patterns.

Table 6
Inter-comparison of well mixed, tidally driven inlet systems along the Southeast Coast of North America. North Inlet, South Carolina (Kjerfve and Proehl, 1979; Kerfve et al., 1981; Kjerfve et al., 1982; Dame et al., 1986; Kjerfve et al., 1991); Beaufort Inlet, North Carolina (Churchill et al., 1999; Hench and Luettich, 2003); Sand Shoal Inlet, Virginia (Li, 2002). Arrows indicate view for bathymetry and flow

Location			Beaufort Inlet, NC	North Inlet, SC	Sand Shoal Inlet, VA	St. Augustine Inlet, FL
Location Map					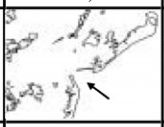	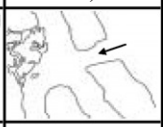
Inlet Bathymetry			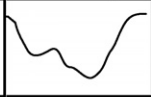	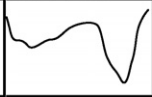		
Residual Circulation			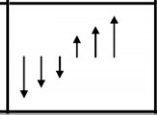	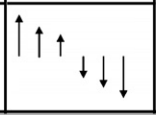	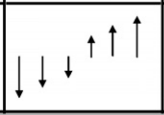	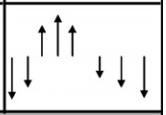
Characteristics						
Well Mixed		Vertical	x	x	x	x
		Horizontal		x	x	x
Tidal Forcing		Constituent	M2	M2	M2	M2
		Variance	-	75%	83%	86%
Tide Propagation		Standing		x	x	x
		Progressive	x			
Governing Dynamics		Local Acceleration	x			
		Advection	x	x	x	x
		Coriolis	x			
		Barotropic P.G.	x	x	x	x
		Baroclinic P.G.				
		Friction	x	x	x	x
Residual Circulation	Net Inflow	Shoals		x		
		Channel	x		x	x
	Net Outflow	Shoals	x		x	x
		Channel		x		

All four systems are classified as well-mixed and tidally driven, and all contain inlet-proximate flow splits. Additionally, the systems share similar forcing mechanisms yet the residual circulation patterns are different. A comparison of Sand Shoal Inlet and St. Augustine Inlet may be the exception: residual circulation and frictional characteristics are similar. Both Sand Shoal (at the western transect) and St. Augustine show net inflow through a deep channel and mean outflow over shoals. Both are characterized by a tidal signal that is roughly 90° out of phase with tidal currents. With the limited amount of information regarding Sand Shoal Inlet, it is difficult to determine if this is a manifestation of the channel length theory of Li and O'Donnell (2005), or Stommel and Farmer's (1952) source–sink analog.

Kjerfve et al. (1982) suggest that North Inlet is representative of a number of estuarine systems along the southeastern seaboard of the United States, ranging from Cape Hatteras, North Carolina to Cape Canaveral, Florida. Two of the other three systems analyzed in Table 6 (St. Augustine Inlet and Beaufort Inlet) lie within this region, but exhibit

different subtidal flow properties. While these systems may share some characteristics, commonalities between subtidal flow patterns are not evident. This suggests that there are unidentified characteristics, such as bathymetry, that make subtidal behavior unique. Qualifying the effects of local bathymetry and morphology on subtidal flow, therefore, may be as important as understanding the degree to which hydrographic properties and forcing mechanisms affect subtidal behavior. This is one area where future efforts should concentrate.

7. Conclusions

Residual circulation at this trifurcation is dominated by tidal rectification from advective acceleration. The contributions of friction and Coriolis appear to be less significant and the baroclinic pressure gradient was weak during the study period. An appropriate subtidal momentum balance for the system, therefore, may be expressed by advection and the barotropic pressure gradient. The observed subtidal flow at St. Augustine Inlet might be described by both the source–sink analog of Stommel and Farmer (1952) and by Li and O'Donnell's (2005) analytical model of residual circulation in a short channel, with mean inflow through the deep channel and mean outflow over the shoals. Four additional findings are also evident from the results: (1) axial convergence fronts and regions of flow divergence existed within the study domain; (2) a freshwater-influenced environment existed offshore; (3) a quasi-standing wave influences the system; (4) and the study domain was vertically well-mixed and surface hydrography was uniform.

Acknowledgments

We are indebted to Messrs. Vik Adams and Sidney Schofield, for expert technical assistance. We gratefully acknowledge the assistance of Ms. Hande Caliskan and Mr. Justin Marin, during data collection. AVL acknowledges support from NSF project 0551923. The authors thank C. Li, D. Huntley, and an anonymous reviewer for insightful suggestions.

References

Atkinson, L.P., Lee, T.N., Blanton, J.O., Chandler, W.S., 1983. Climatology of the Southeastern United States continental shelf waters. Journal of Geophysical Research 88, 4705–4718.

Blanton, J.O., Atkinson, L.P., 1983. Transport and fate of river discharge on the continental shelf of the Southeastern United States. Journal of Geophysical Research 88, 4730–4738.

Chadwick, D.B., Largier, J.L., 1999. Tidal exchange at the bay-ocean boundary. Journal of Geophysical Research 104 (C12), 29901–29924.

Churchill, J.H., Forward, R.B., Luettich, R.A., Hench, J.L., Hettler, W.F., Crowder, L.B., Blanton, J.O., 1999. Circulation and larval fish transport within a tidally dominated estuary. Fisheries Oceanography 8 (2), 173–189.

Dame, R., Chrzanowski, T., Bildstein, K., Kjerfve, B., McKellar, H., Nelson, D., Spurrier, J., Stancyk, S., Stevenson, H., Vernberg, J., Zingmark, R., 1986. The outwelling hypothesis and North Inlet, South Carolina. Marine Ecology Progress Series 33, 217–229.

Dame, R., Alber, M., Allen, D., Mallin, M., Montague, C., Lewitus, A., Chalmers, A., Gardner, R., Gilman, C., Kjerfve, B., Pinckney, J., Smith, N., 2000. Estuaries of the South Atlantic coast of North America: their geographical signatures. Estuaries 23 (6), 793–819.

Fischer, H.B., 1972. Mass transport mechanisms in partially stratified estuaries. Journal of Fluid Mechanics 53, 671–687.

Fischer, H.B., List, E.J., Koh, R.C.Y., Imberger, J., Brooks, N.H., 1979. Mixing in Inland and Coastal Waters. Academic, San Diego, California.

Hansen, D.V., Rattray, M., 1966. New dimensions in estuary classification. Limnology and Oceanography 11, 319–326.

Hench, J.L., Luettich, R.A., 2003. Transient tidal circulation and momentum balances at a shallow inlet. Journal of Physical Oceanography 33, 913–932.

Joyce, T.M., 1989. On in situ calibration of shipboard ADCPs. Journal of Atmospheric Oceanic Technology 6 (1), 169–172.

Kasai, A., Hill, A.E., Fujiwara, T., Simpson, J.H., 2000. Effect of the Earth's rotation on circulation in regions of freshwater influence. Journal of Geophysical Research 105 (C7), 16961–16969.

Kjerfve, B., Proehl, J.A., 1979. Velocity variability in a cross-section of a well-mixed estuary. Journal of Marine Research 37 (3), 409–418.

Kjerfve, B., Stevenson, L.H., Proehl, J.A., Chrzanowski, T.H., Kitchens, W.M., 1981. Estimation of material fluxes in an estuarine cross section: a critical analysis of spatial measurement density and errors. Limnology and Oceanography 26 (2), 325–335.

Kjerfve, B., Proehl, J.A., Schwing, F.B., Seim, H.E., Marozas, M., 1982. Temporal and spatial considerations in measuring estuarine water fluxes. Estuarine Comparisons, 37–51.

Kjerfve, B., Miranda, L.B., Wolanski, E., 1991. Modelling water circulation in an estuary and intertidal salt marsh system. Netherlands Journal of Sea Research 28 (3), 141–147.

Li, C., 2002. Axial convergence fronts in a barotropic tidal inlet—Sand Shoal Inlet, VA. Continental Shelf Research 22, 2633–2653.

Li, C., O'Donnell, J., 2005. The effect of channel length on the residual circulation in tidally dominated channels. Journal of Physical Oceanography 35, 1826–1840.

National Estuarine Research Reserve System (NERRS), 2006. National Oceanic and Atmospheric Administration, Central Data Management Office WWW Page ⟨http://cdmo.baruch.sc.edu⟩.

National Oceanic and Atmospheric Administration (NOAA), 2006. Tides and Currents, WWW Page ⟨http://tidesandcurrents.noaa.gov⟩.

Nunes, R.A., Simpson, J.H., 1985. Axial convergence in a well-mixed estuary. Estuarine Coastal Shelf Science 20, 637–649.

Ott, M.W., Garrett, C., 1998. Frictional estuarine flow in Juan de Fuca Strait, with implications for secondary circulation. Journal of Geophysical Research 103, 15657–15666.

Pritchard, D.W., 1956. The dynamic structure of a coastal plain estuary. Journal of Marine Research 15, 33–42.

Rivière, P., Treguier, A.M., Klein, P., 2004. Effects of bottom friction on nonlinear equilibration of an oceanic baroclinic jet. Journal of Physical Oceanography 34, 416–432.

Sanay, R., Valle-Levinson, A., 2005. Wind-induced circulation in semienclosed homogenous, rotating basins. Journal of Physical Oceanography 35, 2520–2531.

Stommel, H., Farmer, H.G., 1952. On the nature of estuarine circulation. Woods Hole Oceanographic Institute, Woods Hole, Massachusetts Ref. 52–51, 52–63, 52–88.

Valle-Levinson, A., Li, C., Wong, K.C., Lwiza, K.M.M., 2000a. Convergence of lateral flow along a coastal plain estuary. Journal of Geophysical Research 105, 17045–17061.

Valle-Levinson, A., Wong, K.C., Lwiza, K.M.M., 2000b. Fortnightly variability in the transverse dynamics of a coastal plain estuary. Journal of Geophysical Research 105, 3413–3424.

Valle-Levinson, A., Reyes, C., Sanay, R., 2003. Effects of bathymetry, friction, and rotation on estuary-ocean exchange. Journal of Physical Oceanography 33, 2375–2393.

Winant, C.D., 2004. Three-dimensional wind-driven flow in an elongated, rotating basin. Journal of Physical Oceanography 34, 462–476.

Winant, C.D., Gutiérrez de Velasco, G., 2003. Tidal dynamics and residual circulation in a well-mixed inverse estuary. Journal of Physical Oceanography 33, 1365–1379.

Wong, K.C., 1994. On the nature of transverse variability in a coastal plain estuary. Journal of Geophysical Research 99, 14209–14222.

Zimmerman, J.T.F., 1981. Dynamics, diffusion, and geohyphen-qj;morphological significance of tidal eddies. Nature 290, 549–555.